# Electron correlations in a multivalley electron gas and Fermion-boson conversion

Yasutami Takada
*Institute for Solid State Physics, University of Tokyo, 7-22-1 Roppongi, Minato-ku, Tokyo 106, Japan*
(Received 11 April 1990; revised manuscript received 11 June 1990)

The correlation energy $\varepsilon_c$, the chemical-potential shift due to the correlation, $\mu_c$, the compressibility $\kappa$, and the renormalization factor at the Fermi surface, $z_F$, are calculated for the paramagnetic valley-unpolarized state of the multivalley electron gas that may be realized in a doped multivalley semiconductor or multivalley semimetal. The calculations are based on an improved version of the effective-potential expansion method, which is known to give accurate $\varepsilon_c$, $\mu_c$, $\kappa$, and $z_F$ for a single-valley electron gas at metallic densities. The valley degeneracy is found to be a good parameter to connect the total energies of the electron gas of both paramagnetic and ferromagnetic states with that of the charged-boson system. Based on this connection, the possibility of a valley-polarized state is discussed.

## I. INTRODUCTION

Many-body effects in the electron gas have been studied for a long time. By now the ground-state energy of the system is well known at metallic densities. The Green's-function Monte Carlo (GFMC) calculation of Ceperley and Alder[1] played a decisive role in its determination, but other calculations, in particular, the coupled-cluster one by Emrich and Zabolitzky,[2] gave virtually the same result. The effective-potential expansion (EPX) method proposed by the present author could also provide accurately the ground-state energy as well as other quantities such as the pair-distribution function.[3]

In this paper we present an improved version of the EPX method in which the long-range part of the electron correlation can be included better than the previous version in Ref. 3. Since the Coulomb interaction $V(q)$ has a long-range tail, i.e., $V(q) \propto q^{-2}$, this improvement is vital to obtain accurate results for quantities such as the renormalization factor at the Fermi surface. In fact, a prescription of this improvement was already given when superconductivity in the electron gas was discussed,[4] but substantial progress has been made here. We also prove that the static approximation employed in Ref. 4 in the calculation of the short-range part of the electron correlation is valid.

We apply the improved EPX method to a multivalley electron gas, which may be realized in a doped multivalley semiconductor or multivalley semimetal. There are three major reasons for this study. First, many-body effects in the electron gas are usually divided into the exchange and correlation effects, but their relative importance changes with increasing valley degeneracy $g_v$. The correlation effect, especially the one described by the so-called ring diagrams, is expected to dominate in the large-$g_v$ limit with a fixed number of electrons in each valley, but other terms such as those corresponding to the exchange and ladder diagrams are also known to be important in the usual electron gas in which $g_v=1$. Thus it is interesting to know the critical value of $g_v$ at which we can safely neglect terms other than those associated with the ring diagrams. Such a critical value will be determined here. Second, if $2g_v$ were larger than the total number of electrons, the total energy of our system would be equal to that of the charged-boson system. Thus we can connect the results of the boson system[1,5] with those of the fermion system by changing $g_v$ with a fixed total number of electrons. Namely, $g_v$ may be regarded as a parameter to convert the results for fermions into those for bosons. Third, there have been interesting proposals for superconductivity in multivalley systems.[6-8] Since superconductivity is a typical many-body effect, we have to understand the normal state in sufficient detail before we make a reliable prediction for the occurrence of superconductivity.

In Sec. II we specify our model system. In Sec. III we give our trial function for the paramagnetic valley-unpolarized state. An expression for the energy expectation value with respect to our trial function is given in Sec. IV. (Terms higher than first order are shown explicitly in Appendixes A and B.) In Sec. V we give our results for the correlation energy $\varepsilon_c$, the chemical-potential shift due to the correlation, $\mu_c$, the compressibility $\kappa$, and the renormalization factor at the Fermi surface, $z_F$. In Sec. VI our results for $\varepsilon_c$ and $z_F$ are compared with those in the random-phase approximation (RPA) to determine the above-mentioned critical value of $g_v$. The connection with the charged-boson system is discussed in Sec. VII. The possibility of a valley-polarized state is also mentioned. Finally, in Sec. VIII we summarize our results and discuss the problem of superconductivity in the multivalley electron gas. In this paper we use units in which $\hbar=1$.

## II. MULTIVALLEY ELECTRON GAS

We consider a system of $N$ electrons embedded in a uniform positive-charge background. The electrons occupy the bottoms of the $g_v$ equivalent valleys in the con-

 

duction band. The effective mass of the valleys will be denoted by $m^*$. The electrons interact with one another through the Coulomb interaction with the static dielectric constant $\epsilon_0$. All the valley-exchange interactions will be neglected. Then the Hamiltonian of the system is written in second quantization as

$$H=H_0+V \ , \tag{2.1}$$

where

$$H_0=\sum_{\mathbf{k},\sigma}\varepsilon_{\mathbf{k}}C^{\dagger}_{\mathbf{k}\sigma}C_{\mathbf{k}\sigma} \ , \tag{2.2}$$

and

$$V=\tfrac{1}{2}\sum_{\mathbf{q}\ (\neq 0)}\sum_{\mathbf{k},\sigma}\sum_{\mathbf{k}',\sigma'}V(q)C^{\dagger}_{\mathbf{k}+\mathbf{q},\sigma}C^{\dagger}_{\mathbf{k}'-\mathbf{q},\sigma'}C_{\mathbf{k}'\sigma'}C_{\mathbf{k}\sigma} \ , \tag{2.3}$$

with $\varepsilon_{\mathbf{k}}=\mathbf{k}^2/2m^*$ and $V(q)=4\pi e^2/\epsilon_0 q^2$. The volume of the system is taken to be unity. We specify an electron by momentum $\mathbf{k}$, spin $s$ $(=\uparrow,\downarrow)$, and valley $i(=1,2,\ldots,g_v)$, and represent its annihilation operator by $C_{\mathbf{k}\sigma}$ with $\sigma=(i,s)$. We note that the total degeneracy of the system is $2g_v$.

In the absence of the interaction, electrons are equally distributed to all the $g_v$ valleys. In each valley electrons occupy the states from the bottom up to the Fermi momentum $k_F\equiv(3\pi^2N/g_v)^{1/3}$. This is the paramagnetic valley-unpolarized state and will be denoted by $|0\rangle$. In the following we measure momenta and energies in units of $k_F$ and effective rydbergs (Ry$^*$) $m^*e^4/2\epsilon_0^2$, respectively. We define the density parameter $r_s^*$ in terms of this $k_F$ and the effective Bohr radius $\epsilon_0/m^*e^2$ as

$$r_s^*=m^*e^2/\alpha\epsilon_0 k_F \ , \tag{2.4}$$

with $\alpha=(4/9\pi)^{1/3}=0.521$. Then the system can be described by the two parameters $r_s^*$ and $g_v$. The choice of $r_s^*$ for the density parameter is useful when we discuss the effect of $g_v$ with a fixed number of electrons in each valley. For the discussion with a fixed total number of electrons, however, it is more convenient to use the conventional density parameter $r_s\equiv m^*e^2/\alpha\epsilon_0(3\pi^2N)^{1/3}$ rather than $r_s^*$. They are related to each other through

$$r_s^*=g_v^{1/3}r_s \ . \tag{2.5}$$

## III. TRIAL FUNCTION IN THE EPX METHOD

In the presence of the interaction, $|0\rangle$ is no longer a good trial wave function even for the paramagnetic valley-unpolarized state. The effects of the electron correlation should be included. In the EPX method such effects are treated by the introduction of the correlation factor $U(0,-\infty)$ in the definition of a trial function as

$$|\Phi_0\rangle=U(0,-\infty)|0\rangle\equiv\sum_{n=0}^{\infty}\frac{1}{n!}\left[\sum_{m=1}^{\infty}U_m(0,-\infty)\right]^n|0\rangle \ , \tag{3.1}$$

with

$$\begin{aligned}U_m(0,-\infty)=&\frac{(-i)^m}{m!}\int_{-\infty}^{0}e^{0^+t_1}dt_1\cdots\int_{-\infty}^{0}e^{0^+t_m}dt_m\,T[\tilde{V}_l(t_1)\cdots\tilde{V}_l(t_m)]_L\\&+\frac{(-i)^m}{(m-1)!}\int_{-\infty}^{0}e^{0^+t_1}dt_1\cdots\int_{-\infty}^{0}e^{0^+t_m}dt_m\,T[\tilde{V}_s(t_1)\tilde{V}_l(t_2)\cdots\tilde{V}_l(t_m)]_L \ ,\end{aligned} \tag{3.2}$$

where $T$ is the symbol for the time-ordered product in the usual sense, and $\tilde{V}_l(t)$ and $\tilde{V}_s(t)$ are, respectively, defined as

$$\tilde{V}_l(t)=e^{iH_0t}\tilde{V}_l e^{-iH_0t} \ , \tag{3.3}$$

and

$$\tilde{V}_s(t)=e^{iH_0t}\tilde{V}_s e^{-iH_0t} \ , \tag{3.4}$$

with the long- and short-range parts of the effective potential $\tilde{V}_l$ and $\tilde{V}_s$. The subscript $L$ to the square bracket denotes, on the one hand, the instruction to consider only terms in which $m$ $\tilde{V}$'s in the bracket are connected with one another, and on the other hand, it indicates to exclude any term in which $\tilde{V}$'s in the different square brackets are linked. In this choice the electron correlations up to infinite order are included for the long-range part. This treatment is necessary for the correct screening property at $q=0$, namely, to avoid divergences caused by the $q^{-2}$ behavior of the bare Coulomb interaction in the calculations of the quasiparticle properties at the Fermi surface. On the contrary, only the two-electron correlation is considered for the short-range part in order to make calculations tractable. The present choice comes from the following physical observation: While very many electrons are involved in the long-range correlation, the two-electron correlation dominates in the short-range part.

Basically, we use a variational principle to determine both $\tilde{V}_l$ and $\tilde{V}_s$. In order to make the variational procedure easier, we choose the same form for $\tilde{V}_l$ and $\tilde{V}_s$ as that in (2.3) for $V$ with the replacement of $V(q)$ by $\tilde{V}_l(q)$ and $\tilde{V}_s(q)$, respectively. The optimum form for $\tilde{V}_s(q)$ will be determined by the solution of a Euler-Lagrange-type equation as we shall show later, but we give a form for $\tilde{V}_l(q)$ as

$$\tilde{V}_l(q)=V(q)/[\tfrac{1}{2}+\tfrac{1}{2}\exp(q^2/q_c^2)] \ . \tag{3.5}$$

The cutoff momentum $q_c$ is a variational parameter, but its optimum value is explored only in the small-$q$ region to make the contribution from complicated exchange terms small. Note that we gave $\tilde{V}_l(q)$ as $V(q)\exp(-q^2/q_c^2)$ rather than (3.5) in Ref. 4. The obtained total energy does not change so much between the two choices for $\tilde{V}_l(q)$, but (3.5) is found to be a better, if not the best, choice.

## IV. ENERGY EXPECTATION VALUE

The energy expectation value $E_0$ with respect to $|\Phi_0\rangle$ can be expanded in the effective potentials $\tilde{V}_l$ and $\tilde{V}_s$ with the use of the generalized linked-cluster theorem.[9,10] In powers of $\tilde{V}_s$, we have

$$E_0 \equiv \frac{\langle \Phi_0|H|\Phi_0\rangle}{\langle \Phi_0|\Phi_0\rangle} = \sum_{n=0}^{\infty} E^{(n)} , \tag{4.1}$$

where $E^{(n)}$ is the $n$th-order term in $\tilde{V}_s$, but it can still be expanded in $\tilde{V}_l$ up to infinite order.

### A. Zeroth-order terms

The terms included in $E^{(0)}$ are represented in Fig. 1 with the use of Feynman diagrams. The Hartree-Fock terms $E_{\rm HF} \equiv \langle 0|H|0\rangle$ are shown in Fig. 1(a), and the ring terms in Fig. 1(b) are calculated as

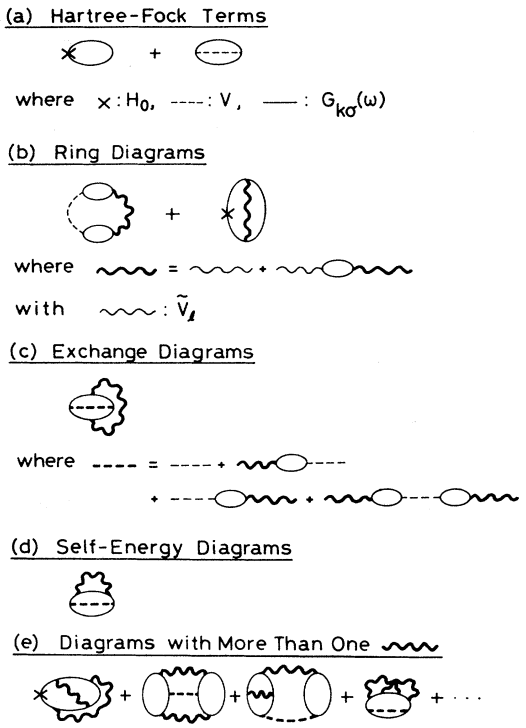


FIG. 1. Feynman diagrams for the terms in $E^{(0)}$.

$$E_r^{(0)}(V) = -\frac{1}{2}\sum_{\mathbf{q}} \int_{-\infty}^{\infty} \frac{d\Omega}{2\pi i} \frac{[\Pi(q,\Omega)]^2 V(q)\tilde{V}_l(q)}{\epsilon(q,\Omega)} , \tag{4.2}$$

and

$$E_r^{(0)}(H_0) = -\sum_{\mathbf{q}}\sum_{\mathbf{k},\sigma} \int_{-\infty}^{\infty} \frac{d\Omega}{2\pi i} \int_{-\infty}^{\infty} \frac{d\omega}{2\pi i} \frac{\tilde{V}_l(q)}{\epsilon(q,\Omega)} \varepsilon_{\mathbf{k}} [G_{\mathbf{k}\sigma}(\omega)]^2 G_{\mathbf{k}+\mathbf{q}\sigma}(\omega+\Omega)$$

$$= \frac{1}{2}\sum_{\mathbf{q}} \int_{-\infty}^{\infty} \frac{d\Omega}{2\pi i} \left[ \ln[\epsilon(q,\Omega)] - \frac{\Pi(q,\Omega)\tilde{V}_l(q)}{\epsilon(q,\Omega)} \right] , \tag{4.3}$$

where $G_{\mathbf{k}\sigma}(\omega)$ is the single-particle Green's function in the noninteracting system, and the dielectric function $\epsilon(q,\Omega)$ is defined through the polarization function $\Pi(q,\Omega)$ in the RPA as

$$\epsilon(q,\Omega) = 1 + \Pi(q,\Omega)\tilde{V}_l(q) . \tag{4.4}$$

In the numerical evaluation of (4.2) and (4.3), it is more convenient to perform the $\Omega$ integral along the imaginary axis rather than the real axis.[11] On the imaginary axis, $\Pi(q,i\Omega)$ is calculated as

$$\Pi(q,i\Omega) = 2\sum_{\mathbf{k},\sigma} \frac{n_{\mathbf{k}\sigma}(1-n_{\mathbf{k}+\mathbf{q},\sigma})\Delta(\mathbf{k};\mathbf{q})}{\Omega^2 + [\Delta(\mathbf{k};\mathbf{q})]^2} , \tag{4.5}$$

where $n_{\mathbf{k}\sigma} \equiv \theta(k_F - |\mathbf{k}|)$ is the momentum distribution function of a free-electron system, and $\Delta(\mathbf{k};\mathbf{q})$ is defined as

$$\Delta(\mathbf{k};\mathbf{q}) \equiv |\varepsilon_{\mathbf{k}+\mathbf{q}} - \varepsilon_{\mathbf{k}}| . \tag{4.6}$$

The sum of (4.2) and (4.3) is of the order of 10 mRy* per electron, and those ring terms are predominantly important for $\tilde{V}_l(q)$ which is not zero only for small $q$. In fact, all the exchange and self-energy terms were neglected in Ref. 4, in which the cutoff momentum $q_c$ was restricted to the region of $0 < q_c < 0.1k_F$. In this paper, however, we include the terms (c) and (d) in Fig. 1 in order to explore the optimum $q_c$ in a wider range. The contributions from other terms having at least two thick wavy interactions shown in Fig. 1(e) are estimated and found to have values (mostly much) less than 0.01 mRy* per electron for any $r_s^*$ and $g_v$ considered here if $q_c$ is less than $0.3k_F$. Thus we neglect them and

search an optimum value for $q_c$ in the region of $0<q_c<0.3k_F$.

The exchange term (c) is expressed as

$$E_{\rm ex}^{(0)}(V)=\frac{1}{2}\sum_{\mathbf{q},\mathbf{q}'}\sum_{\mathbf{k},\sigma}\int_{-\infty}^{\infty}\frac{d\Omega}{2\pi i}\int_{-\infty}^{\infty}\frac{d\Omega'}{2\pi i}\int_{-\infty}^{\infty}\frac{d\omega}{2\pi i}\frac{\tilde{V}_l(q)}{\epsilon(q,\Omega)}\frac{V(q')}{[\epsilon(q',\Omega')]^2}$$
$$\times G_{\mathbf{k}\sigma}(\omega)G_{\mathbf{k}+\mathbf{q}',\sigma}(\omega+\Omega')G_{\mathbf{k}+\mathbf{q},\sigma}(\omega+\Omega)G_{\mathbf{k}+\mathbf{q}+\mathbf{q}',\sigma}(\omega+\Omega+\Omega')\ . \tag{4.7}$$

Before performing the $\Omega'$ integration, we expand $V(q')/[\epsilon(q',\Omega')]^2$ in terms of $\Delta\Pi(q',\Omega')\equiv\Pi(q',\Omega')-\Pi(q',0)$ as

$$\frac{V(q')}{[\epsilon(q',\Omega')]^2}=\bar{V}(q')-2\bar{V}(q')\frac{\tilde{V}_l(q')}{\epsilon(q',0)}\Delta\Pi(q',\Omega')+\cdots\ , \tag{4.8}$$

where

$$\bar{V}(q)\equiv\frac{V(q)}{[\epsilon(q,0)]^2}\ . \tag{4.9}$$

Because $\bar{V}(q)$ becomes very small for small $q$ while $\tilde{V}_l(q)/\epsilon(q,0)$ remains finite only in such a region of $q$, the product of these two interactions is always small in the whole $q$ region. An example of the values of this product is shown in Fig. 2 for the case of $r_s^*=5$ and $g_v=1$. Such a product appears in all the terms except the first one in the expansion (4.8). Thus we can neglect those terms and may replace $V(q')/[\epsilon(q',\Omega')]^2$ by $\bar{V}(q')$ in (4.7). This is nothing but the static approximation employed in Ref. 4, but no justification of it was given there. Unfortunately, the same argument cannot be applied to $\tilde{V}_l(q)/\epsilon(q,\Omega)$, and we have to perform the $\Omega$ integration as it is in (4.7). By changing the integral along the imaginary axis, we can rewrite (4.7) as

$$E_{\rm ex}^{(0)}(V)=\sum_{\mathbf{q},\mathbf{q}'}\sum_{\mathbf{k},\sigma}\int_0^{\infty}\frac{d\Omega}{\pi}\frac{\tilde{V}_l(q)}{\epsilon(q,i\Omega)}\bar{V}(q')n_{\mathbf{k}\sigma}(1-n_{\mathbf{k}+\mathbf{q},\sigma})$$
$$\times\left[n_{\mathbf{k}+\mathbf{q}+\mathbf{q}',\sigma}(1-n_{\mathbf{k}+\mathbf{q}',\sigma})\frac{\Omega^2+\Delta(\mathbf{k};\mathbf{q})\Delta(\mathbf{k}+\mathbf{q}';\mathbf{q})}{\{\Omega^2+[\Delta(\mathbf{k};\mathbf{q})]^2\}\{\Omega^2+[\Delta(\mathbf{k}+\mathbf{q}';\mathbf{q})]^2\}}\right.$$
$$\left.+n_{\mathbf{k}+\mathbf{q}',\sigma}(1-n_{\mathbf{k}+\mathbf{q}+\mathbf{q}',\sigma})\frac{-\Omega^2+\Delta(\mathbf{k};\mathbf{q})\Delta(\mathbf{k}+\mathbf{q}';\mathbf{q})}{\{\Omega^2+[\Delta(\mathbf{k};\mathbf{q})]^2\}\{\Omega^2+[\Delta(\mathbf{k}+\mathbf{q}';\mathbf{q})]^2\}}\right]\ . \tag{4.10}$$

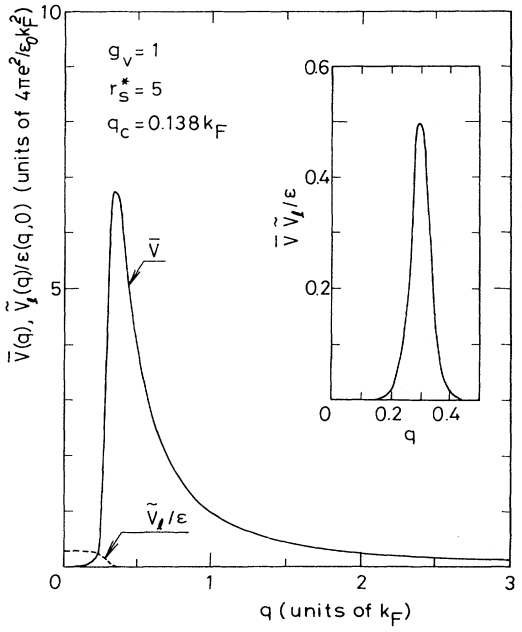


FIG. 2. Example for the values of $\bar{V}(q)$ and $\tilde{V}_l(q)/\epsilon(q,0)$ in units of $4\pi e^2/\epsilon_0 k_F^2$ as a function of $q$. The inset shows the product of the two functions. The case of $r_s^*=5$ and $g_v=1$ is shown.

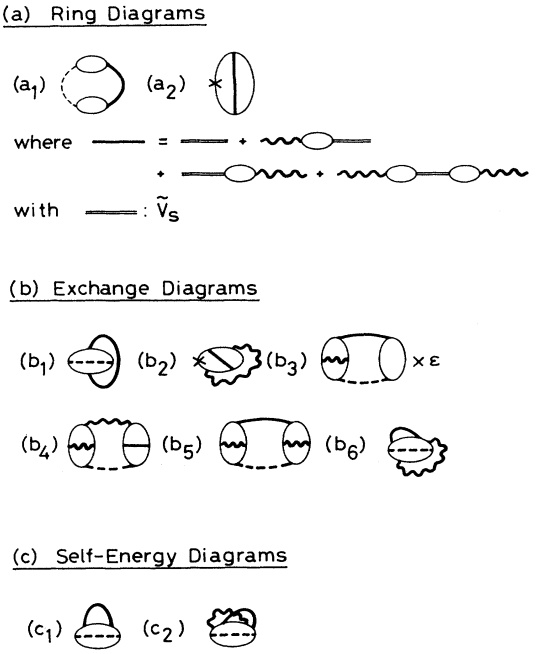


FIG. 3. Feynman diagrams for the terms in $E^{(1)}$.

By a similar argument, we obtain the self-energy term (d) as

$$E_s^{(0)}(V)=\sum_{\mathbf{q},\mathbf{q}'}\sum_{\mathbf{k},\sigma}\int_0^\infty\frac{d\Omega}{\pi}\frac{\tilde{V}_l(q)}{\epsilon(q,i\Omega)}\bar{V}(q')n_{\mathbf{k}\sigma}(1-n_{\mathbf{k}+\mathbf{q},\sigma})(n_{\mathbf{k}+\mathbf{q}+\mathbf{q}',\sigma}-n_{\mathbf{k}+\mathbf{q}',\sigma})\frac{-\Omega^2+[\Delta(\mathbf{k};\mathbf{q})]^2}{\{\Omega^2+[\Delta(\mathbf{k};\mathbf{q})]^2\}^2}\ . \tag{4.11}$$

Evaluated values of (4.10) and (4.11) are less than 0.4 mRy* per electron.

### B. First-order terms

In Fig. 3 we show some of the terms in $E^{(1)}$ by Feynman diagrams. The ring terms ($a_1$) and ($a_2$) can be combined into

$$E_r^{(1)}(V)+E_r^{(1)}(H_0)=-\frac{1}{2}\sum_{\mathbf{q}}\int_{-\infty}^{\infty}\frac{d\Omega}{2\pi i}[V(q)-\tilde{V}_l(q)]\frac{\tilde{V}_s(q)}{[\epsilon(q,\Omega)]^2}[\Pi(q,\Omega)]^2\ . \tag{4.12}$$

As in (4.7), we expand $\tilde{V}_s(q)/[\epsilon(q,\Omega)]^2$ in terms of $\Delta\Pi(q,\Omega)\equiv\Pi(q,\Omega)-\Pi(q,0)$. Since $\tilde{V}_s(q)$ is at most $V(q)$, we can repeat exactly the same argument as that following (4.9) to show smallness of the product of $\bar{V}_s(q)$ and $\tilde{V}_l(q)/\epsilon(q,0)$, where $\bar{V}_s(q)$ is defined as

$$\bar{V}_s(q)\equiv\frac{\tilde{V}_s(q)}{[\epsilon(q,0)]^2}\ . \tag{4.13}$$

Thus we may replace $\tilde{V}_s(q)/\epsilon(q,\Omega)^2$ by $\bar{V}_s(q)$ in (4.12), and we can perform the $\Omega$ integration in (4.12) easily to obtain

$$E_r^{(1)}(V)+E_r^{(1)}(H_0)=-\sum_{\mathbf{q}}\sum_{\mathbf{k},\sigma}\sum_{\mathbf{k}',\sigma'}[V(q)-\tilde{V}_l(q)]\bar{V}_s(q)\frac{n_{\mathbf{k}\sigma}(1-n_{\mathbf{k}+\mathbf{q},\sigma})n_{\mathbf{k}'\sigma'}(1-n_{\mathbf{k}'-\mathbf{q},\sigma'})}{\Delta(\mathbf{k};\mathbf{q})+\Delta(\mathbf{k}';-\mathbf{q})}\ . \tag{4.14}$$

This is the expression (4.5) in Ref. 4 derived in the static approximation. This term has a value larger than 100 mRy* per electron and gives the largest contribution to the correlation energy.

The same argument is applied to the term ($b_1$) in Fig. 3 to obtain

$$E_{\rm ex}^{(1)}(V)=\sum_{\mathbf{q}}\sum_{\mathbf{k},\sigma}\sum_{\mathbf{k}',\sigma'}\delta_{\sigma\sigma'}\bar{V}_s(q)\bar{V}(|\mathbf{k}'-\mathbf{k}-\mathbf{q}|)\frac{n_{\mathbf{k}\sigma}(1-n_{\mathbf{k}+\mathbf{q},\sigma})n_{\mathbf{k}'\sigma'}(1-n_{\mathbf{k}'-\mathbf{q},\sigma'})}{\Delta(\mathbf{k};\mathbf{q})+\Delta(\mathbf{k}';-\mathbf{q})}\ . \tag{4.15}$$

with $\delta_{\sigma\sigma'}\equiv\delta_{ii'}\delta_{ss'}$. This exchange term has the absolute value of about $(3g_v)^{-1}$ of that of (4.14). Another exchange term ($b_2$) in Fig. 3 is given by

$$\begin{aligned}E_{\rm ex}^{(1)}(H_0)=-2\sum_{\mathbf{q},\mathbf{q}'}\sum_{\mathbf{k},\sigma}\int_0^\infty\frac{d\Omega}{\pi}\frac{\tilde{V}_l(q)}{\epsilon(q,i\Omega)}\bar{V}_s(q')n_{\mathbf{k}\sigma}(1-n_{\mathbf{k}+\mathbf{q},\sigma})\\ \times\Bigg[n_{\mathbf{k}+\mathbf{q}+\mathbf{q}',\sigma}(1-n_{\mathbf{k}+\mathbf{q}',\sigma})\Bigg\{\frac{\Delta(\mathbf{k};\mathbf{q})\Delta(\mathbf{k}+\mathbf{q}';\mathbf{q})}{\{\Omega^2+[\Delta(\mathbf{k};\mathbf{q})]^2\}\{\Omega^2+[\Delta(\mathbf{k}+\mathbf{q}';\mathbf{q})]^2\}}\\ +[\Delta(\mathbf{k};\mathbf{q})-\Delta(\mathbf{k}+\mathbf{q}';\mathbf{q})]^2\\ \times\frac{\Omega^2[\Omega^2-\Delta(\mathbf{k};\mathbf{q})\Delta(\mathbf{k}+\mathbf{q}';\mathbf{q})]}{\{\Omega^2+[\Delta(\mathbf{k};\mathbf{q})]^2\}^2\{\Omega^2+[\Delta(\mathbf{k}+\mathbf{q}';\mathbf{q})]^2\}^2}\Bigg\}\\ +n_{\mathbf{k}+\mathbf{q}',\sigma}(1-n_{\mathbf{k}+\mathbf{q}+\mathbf{q}',\sigma})\Bigg\{\frac{\Delta(\mathbf{k};\mathbf{q})\Delta(\mathbf{k}+\mathbf{q}';\mathbf{q})}{\{\Omega^2+[\Delta(\mathbf{k};\mathbf{q})]^2\}\{\Omega^2+[\Delta(\mathbf{k}+\mathbf{q}';\mathbf{q})]^2\}}\\ -[\Delta(\mathbf{k};\mathbf{q})+\Delta(\mathbf{k}+\mathbf{q}';\mathbf{q})]^2\\ \times\frac{\Omega^2[\Omega^2+\Delta(\mathbf{k};\mathbf{q})\Delta(\mathbf{k}+\mathbf{q}';\mathbf{q})]}{\{\Omega^2+[\Delta(\mathbf{k};\mathbf{q})]^2\}^2\{\Omega^2+[\Delta(\mathbf{k}+\mathbf{q}';\mathbf{q})]^2\}^2}\Bigg\}\Bigg]\ .\end{aligned} \tag{4.16}$$

This term has the absolute value of about 0.2 mRy* per electron.

The term ($b_3$) in Fig. 3 is written as

$$\begin{aligned}E_{\rm ex'}^{(1)}(V)=-\sum_{\mathbf{q},\mathbf{q}'}\sum_{\mathbf{k},\sigma}\int_{-\infty}^{\infty}\frac{d\Omega}{2\pi i}\int_{-\infty}^{\infty}\frac{d\Omega'}{2\pi i}\int_{-\infty}^{\infty}\frac{d\omega}{2\pi i}\frac{\tilde{V}_l(q)}{\epsilon(q,\Omega)}\frac{\tilde{V}_s(q')V(q')\Pi(q',\Omega')}{[\epsilon(q',\Omega')]^3}\\ \times G_{\mathbf{k}\sigma}(\omega)G_{\mathbf{k}+\mathbf{q}',\sigma}(\omega+\Omega')G_{\mathbf{k}+\mathbf{q},\sigma}(\omega+\Omega)G_{\mathbf{k}+\mathbf{q}+\mathbf{q}',\sigma}(\omega+\Omega+\Omega')\ .\end{aligned} \tag{4.17}$$

The symbol "$\times\epsilon$" in the diagram ($b_3$) indicates that we should multiply $\epsilon(q',\Omega')$ in the final expression to avoid the double counting of the screening factor. Thus $[\epsilon(q',\Omega')]^3$ instead of $[\epsilon(q',\Omega')]^4$ appears in (4.17). We find that this fac-

tor can be replaced by $[\epsilon(q',0)]^3$. The evaluated value of the term (4.17) is about the same as that of $E_{ex}^{(1)}(H_0)$. However, the contribution of this term is mostly canceled by those of the diagrams ($b_4$) and ($b_5$) in Fig. 3, which are the exchange partners to the term ($b_3$). Thus the term ($b_3$) can be neglected together with those of ($b_4$) and ($b_5$). We can also show that the self-energy term ($c_1$), given by

$$E_s^{(1)}(V)=\sum_{\mathbf{q},\mathbf{q}'}\sum_{\mathbf{k},\sigma}\int_{-\infty}^{\infty}\frac{d\Omega}{2\pi i}\int_{-\infty}^{\infty}\frac{d\Omega'}{2\pi i}\int_{-\infty}^{\infty}\frac{d\omega}{2\pi i}\frac{\tilde{V}_s(q)}{[\epsilon(q,\Omega)]^2}\frac{V(q')}{[\epsilon(q',\Omega')]^2}[G_{\mathbf{k}\sigma}(\omega)]^2 G_{\mathbf{k}+\mathbf{q}',\sigma}(\omega+\Omega')G_{\mathbf{k}+\mathbf{q},\sigma}(\omega+\Omega)\ , \tag{4.18}$$

can be neglected. If we expand $\tilde{V}_s(q)/[\epsilon(q,\Omega)]^2$ and $V(q')/[\epsilon(q',\Omega')]^2$ as in (4.8), the leading term of (4.18) vanishes exactly. The next terms are almost canceled by the exchange terms ($c_2$) and ($b_6$). By a similar argument, we find that the contribution from all the other first-order terms is very small. From the experience of evaluating these terms, we find it safe to neglect the ring-exchange diagrams in which $\tilde{V}_l$ connects two electron lines in one polarization bubble. All those ring-exchange diagrams will not be considered in higher-order terms from the outset.

### C. Second-order terms

Since $\tilde{V}_s$ enters into the correlation factor in (3.2) in a different way from $\tilde{V}_l$, the Goldstone diagrams are more convenient than the Feynman ones to express the second- and higher-order terms. In Fig. 4 we give all the important second-order topologically different diagrams. (Only one term among topologically equivalent diagrams is shown.) The static approximation to the dielectric function $\epsilon$ is found to be valid in the terms in Fig. 4. Then the actual expansion parameter is $\bar{V}_s(q)$ rather than $\tilde{V}_s(q)$. For this interaction $\bar{V}_s(q)$, all the direct terms are accompanied by its exchange partners. Thus the Pauli principle is satisfied order by order for the short-range part of the correlation. An explicit expression for each diagram is given in Appendix A.

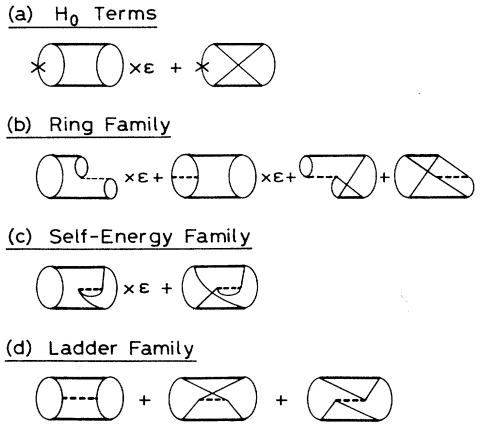


FIG. 4. Goldstone diagrams for the terms in $E^{(2)}$.

### D. Determination of the effective potentials

In all the terms so far considered, $\bar{V}_s(q)$ instead of $\tilde{V}_s(q)$ appears. This function is not large for any $q$: For large $q$, $\bar{V}_s(q)$ is at most $V(q)$ and is small. For small $q$, $\bar{V}_s(q)$ is also small because of the screening factor in (4.13). Thus $\bar{V}_s(q)$ is a good expansion parameter in the whole region of $q$. If it is a small parameter, we can obtain a reasonably good value for $\bar{V}_s(q)$ even if we neglect all the terms higher than second order in (4.1) in the solution of the Euler-Lagrange-type equation

$$\frac{\delta E_0}{\delta \bar{V}_s(q)}=0\ . \tag{4.19}$$

We solve (4.19) numerically with all the terms mentioned in Secs. IV A–IV C for each value of $q_c$ in (3.5). We then calculate $E_0$ to this order and search an optimum value for $q_c$. In Figs. 5(a) and 5(b) we plot the results of $\bar{V}_s$ as a function of $q$ for $r_s^*=1$, 3, and 5, and $g_v=1$ and 4. As expected, $\bar{V}_s(q)$ is reduced much from the bare potential $V(q)$ shown by the dotted curve. The optimum values for $q_c$ are given in Fig. 5(c) as a function of $r_s^*$ for various $g_v$. The values of $\tilde{V}_l(q)/\epsilon(q,0)$ are also shown by the dashed curves in Figs. 5(a) and 5(b). We can see a crossover from $\tilde{V}_l(q)$ to $\tilde{V}_s(q)$ to treat the correlation effect with the increase of $q$. Note that (4.19) reduces to the Bethe-Salpeter equation in the ladder approximation for large $q$.[12,13]

### E. Higher-order terms

As can be seen in Figs. 5(a) and 5(b), the obtained $\bar{V}_s(q)$ has its maximum at $q$ around $0.5k_F$. This indicates that the contribution of higher-order ring and self-energy families may not be neglected. The reasoning used to select the important diagrams in the third- and fourth-order terms was given in Sec. III of Ref. 3, and it will not be repeated here. After appropriate screening factors with respect to $\epsilon$ are included and some simplification is made for some of the exchange terms,we obtain the expressions for these terms, which are given in Appendix B. (The static approximation for $\epsilon$ is also found to be valid in these terms.) We evaluate these ring, the ring-exchange, and self-energy diagrams up to eighth order with $\bar{V}_s(q)$ determined in Sec. IV D.

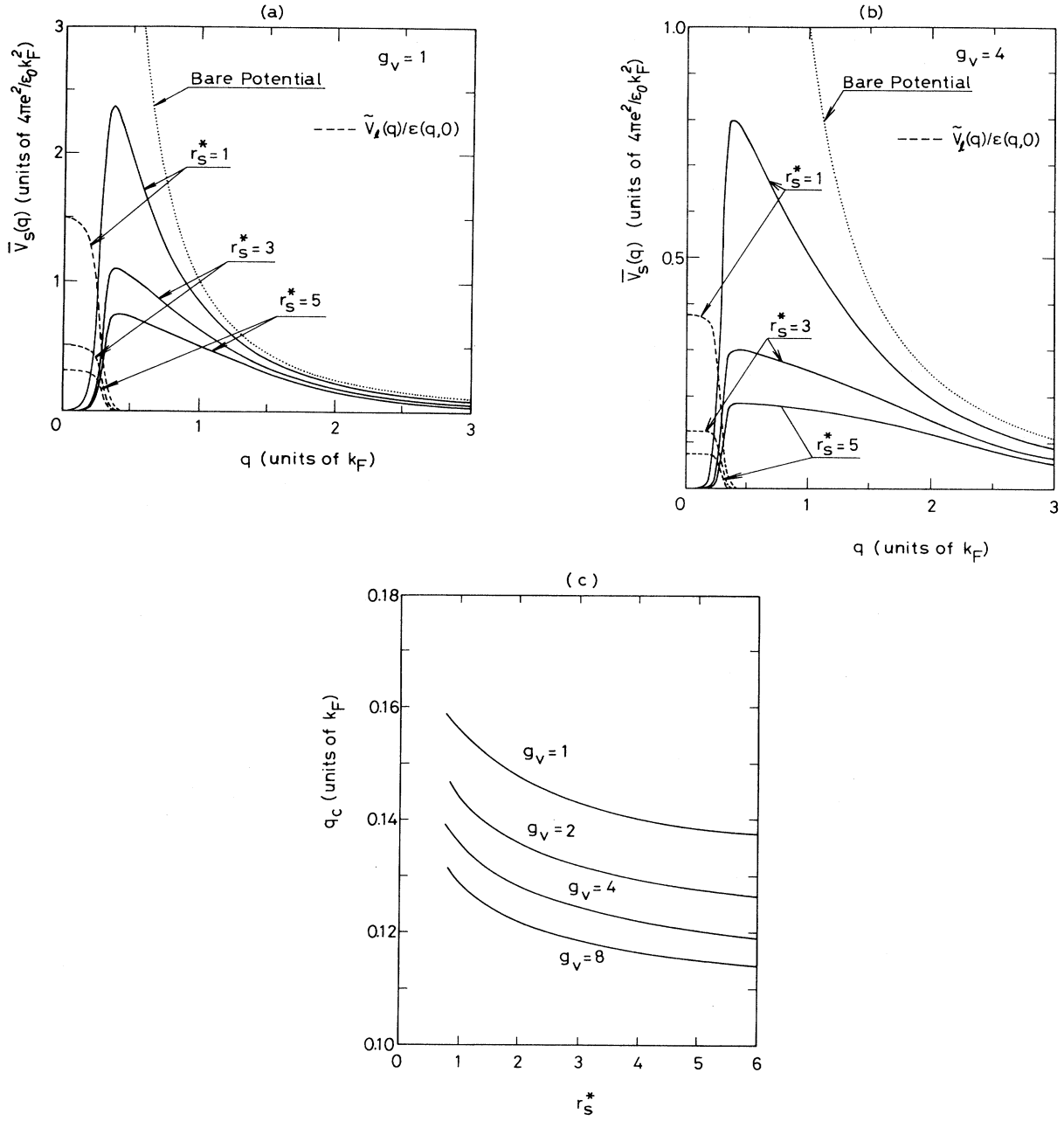


FIG. 5. Calculated results for the short-range part of the effective potential $\bar{V}_s(q)$ in units of $4\pi e^2/\epsilon_0 k_F^2$ are shown as a function of $q$ for $r_s^* = 1$, 3, and 5 in (a) and (b) for $g_v = 1$ and 4, respectively. For comparison, $\tilde{V}_l(q)/\epsilon(q,0)$ and the bare potential $V(q)$ are, respectively, shown by the dashed and dotted curves in each figure. The optimum values for $q_c$ are plotted in (c) as a function of $r_s^*$ for $g_v = 1$, 2, 4, and 8.

## V. CALCULATED RESULTS

In Fig. 6 the correlation energy per electron $\varepsilon_c \equiv (E_0 - E_{\rm HF})/N$ in Ry* units is shown as a function of $r_s^*$ for $g_v = 1$. The results with all the terms up to second order in $\bar{V}_s$ are plotted by the dashed curve and those with terms up to fourth and sixth orders explained in Sec. IV E are, respectively, given by the dotted and solid curves. The effect of the eighth-order terms is also evaluated and found to be small. Thus the results converge by sixth order for $g_v = 1$. As $g_v$ is increased, the series does not converge so quickly. Thus the results up to eighth order are extrapolated to obtain the final values for $\varepsilon_c$ for $g_v \geq 4$. In Table I we give those values for $\varepsilon_c$. For comparison, we also show the data for $g_v = 1$ from the GFMC (Refs. 1 and 14) and coupled-cluster[2] methods, together with those in the second-order calculation in our method. We admit that our results for $\varepsilon_c$ become less reliable with the increase of $r_s^*$ and/or $g_v$ because of the slower convergence. Thus some other method is necessary to obtain

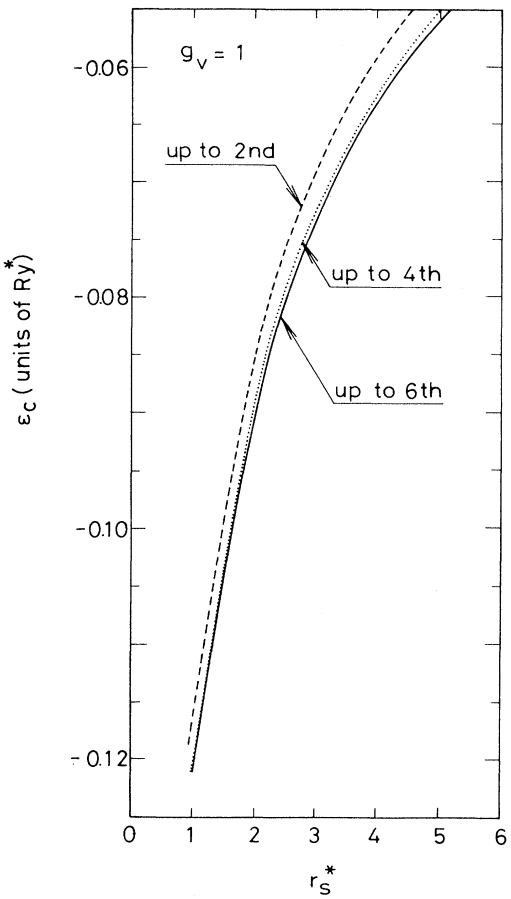


FIG. 6. Calculated correlation energy per electron $\varepsilon_c$ as a function of $r_s^*$ in Ry* units for the case of $g_v=1$. The dashed, dotted, and solid curves represent, respectively, the results with the terms up to second, fourth, and sixth order in $\bar{V}_s$.

$\varepsilon_c$ for $r_s^* \gg 1$ and/or $g_v \gg 1$.

To calculate the chemical potential shift due to the correlation $\mu_c \equiv \varepsilon_c - (r_s^*/3)(\partial\varepsilon_c/\partial r_s^*)$, we need the derivative of $\varepsilon_c$ with respect to $r_s^*$. For this purpose we use an interpolation scheme similar to that introduced in Ref. 14. Let us assume that $\varepsilon_c$ is approximated well by the integral as

$$\varepsilon_c(r_s^*) = -2A\int_0^{(r_s^*)^{-1/2}} dt \frac{t(t+b_0)}{t^3+b_1t^2+b_2t+b_3} . \quad (5.1)$$

We can take the parameter $A$ as $0.062\,1814 g_v$ to reproduce the high-density value of $\varepsilon_c$ [i.e., $\varepsilon_c \to 2(1-\ln 2)/\pi^2 g_v \ln r_s^*$ as $r_s^* \to 0$]. In Ref. 14 other parameters $b_0$, $b_1$, $b_2$, and $b_3$ were determined to reproduce the values for $\varepsilon_c$ of the GFMC at $r_s^*=10$, 20, 50, and 100 for $g_v=1$. The results were given as $b_0=b_1=9.813\,79$, $b_2=2.822\,24$, and $b_3=0.736\,411$. Unfortunately, there are no data available for $\varepsilon_c$ at such large values of $r_s^*$ for $g_v \geq 2$ at present. Thus we take the following procedure: At very low densities (i.e., $r_s \to \infty$), interacting electrons behave like classical particles. Thus the total energy depends only on $r_s$. Namely, $E_0/N$ approaches $-1.792/r_s$ Ry*,[15] irrespective of $g_v$. This result is reproduced if we take the ratio $b_0/b_3$ as $(1.792 g_v^{1/3} - 0.9163)/A$. The remaining parameters $b_1$, $b_2$, and $b_3$ are determined to fit the values of $\varepsilon_c$ at $r_s^*=1$, 2, 3, 4, and 5 obtained in this paper. This is done even for $g_v=1$ to check our procedure. The obtained values of $b_1$, $b_2$, and $b_3$ are given in Table II for various $g_v$. To give some idea about the accuracy of the present procedure, we also give the results of $\varepsilon_c$ in (5.1) together with those for $g_v=1$ in the GFMC method at $r_s^*=10$, 20, and 50. It is seen that our procedure works rather well. The error becomes about 2% even at $r_s^*=50$.

By taking the derivatives of (5.1), we can easily obtain both $\mu_c$ and the compressibility $\kappa$, which is given by

$$\frac{\kappa_F}{\kappa} = 1 - 0.166 r_s^* + 0.0452 r_s^{*3}\left[ r_s^* \frac{\partial^2 \varepsilon_c}{\partial r_s^{*2}} - 2\frac{\partial \varepsilon_c}{\partial r_s^*} \right] , \quad (5.2)$$

with $\kappa_F \equiv (3m^*/N)(g_v/3\pi^2 N)^{2/3}$. The results of $\mu_c$ are given in Fig. 7 as a function of $r_s^*$ for various $g_v$. These values are always much larger (or much smaller in the absolute values) than those in the RPA $\mu_c$(RPA). However, for $g_v \geq 4$, $\mu_c$ is found to be approximately given by the sum of $\mu_c$(RPA) and 0.0484. (The values of the sum are plotted by the dashed curves.) The calculated results of $\kappa_F/\kappa$ are shown in Fig. 8, and they are always smaller than those in the Hartree-Fock approximation [the first two terms in (5.2)]. Namely, the correlation effect makes the system more compressible. Since the correlation effect increases with $g_v$, $\kappa$ becomes larger as $g_v$ is increased. The RPA gives a little larger values for $\kappa$, but the difference becomes very small for large $g_v$. Virtually no difference can be seen for $g_v \geq 4$.

TABLE I. Correlation energy per electron in Ry* units. The columns indicated by GFMC, (GFMC), and CC show, respectively, the results for $g_v=1$ given by the GFMC method by Ceperley and Alder (Ref. 1), the interpolation formula of the GFMC data by Vosko, Wilk, and Nusair (Ref. 14), and the coupled-cluster formalism by Emrich and Zabolitzky (Ref. 2). The fourth to seventh columns give our final results for $g_v=1$, 2, 4, and 6, respectively. (Numbers in parentheses represent our second-order results.)

| $r_s^*$ | GFMC | (GFMC) | CC | $g_v=1$ | $g_v=2$ | $g_v=4$ | $g_v=6$ |
|---|---|---|---|---|---|---|---|
| 1 | −0.119 | −0.120 | −0.122 | −0.121(−0.117) | −0.211(−0.200) | −0.332(−0.310) | −0.421(−0.387) |
| 2 | −0.0902 | −0.0896 | −0.0904 | −0.0899(−0.0855) | −0.152(−0.142) | −0.230(−0.211) | −0.286(−0.257) |
| 3 | | −0.0738 | −0.0738 | −0.0738(−0.0695) | −0.122(−0.113) | −0.180(−0.163) | −0.221(−0.196) |
| 4 | | −0.0636 | −0.0634 | −0.0634(−0.0593) | −0.103(−0.0944) | −0.149(−0.134) | −0.182(−0.160) |
| 5 | −0.0563 | −0.0563 | −0.0560 | −0.0561(−0.0520) | −0.0891(−0.0816) | −0.128(−0.114) | −0.155(−0.136) |

TABLE II. Parameters $b_1$, $b_2$, and $b_3$ in (5.1) for the approximate evaluation of $\varepsilon_c$ for various $g_v$. Results of $\varepsilon_c$ in this approximate formula are shown at $r_s^*=10$, 20, and 50. The results of $\varepsilon_c$ for $g_v=1$ in the GFMC method (Ref. 1) are also given in the column indicated by GFMC for comparison.

| | GFMC | $g_v=1$ | $g_v=2$ | $g_v=4$ | $g_v=6$ | $g_v=8$ |
|---|---|---|---|---|---|---|
| $b_1$ | | 9.905 | 3.249 | 1.192 | 0.7879 | 0.5620 |
| $b_2$ | | 3.256 | 2.528 | 1.741 | 1.478 | 1.292 |
| $b_3$ | | 0.7309 | 0.4315 | 0.2381 | 0.1752 | 0.1368 |
| $\varepsilon_c(r_s^*=10)$ | −0.03722 | −0.0372 | −0.0573 | −0.0811 | −0.0973 | −0.112 |
| $\varepsilon_c(r_s^*=20)$ | −0.02300 | −0.0233 | −0.0350 | −0.0489 | −0.0582 | −0.0662 |
| $\varepsilon_c(r_s^*=50)$ | −0.01140 | −0.0116 | −0.0172 | −0.0238 | −0.0283 | −0.0319 |

The momentum distribution function $n(k)$ is defined as

$$n(k)=\frac{\langle\Phi_0|C_{k\sigma}^{\dagger}C_{k\sigma}|\Phi_0\rangle}{\langle\Phi_0|\Phi_0\rangle}=\sum_{n=0}^{\infty}n^{(n)}(k)\ , \tag{5.3}$$

and the terms in (5.3) can be represented by the same diagrams as those for the expectation value of $H_0$ (the symbol "×") in Sec. IV. We will show in a following paper[16] that our results for $n(k)$ are as accurate as those for $\varepsilon_c$. In Table III we show the results of the renormalization factor at the Fermi surface $z_F$ obtained from the magnitude of the discontinuity of $n(k)$ at $k=k_F$. (Numbers in parentheses are the values in the RPA, as shall be explained in Sec. VI.) With the increase of $g_v$, $z_F$ becomes larger. This indicates a sharper Fermi surface. However, the number of electrons excited from deep inside of the Fermi sphere to the outside of it is increased with $g_v$ as shown in Fig. 9 in which $n(k)$ is plotted for $g_v=1$, 2, and 4 at $r_s^*=3$. Since such excitations are related to the short-range correlation effect, this behavior of $n(k)$ indicates that the important range of the correlation effect becomes shorter with the increase of $g_v$.

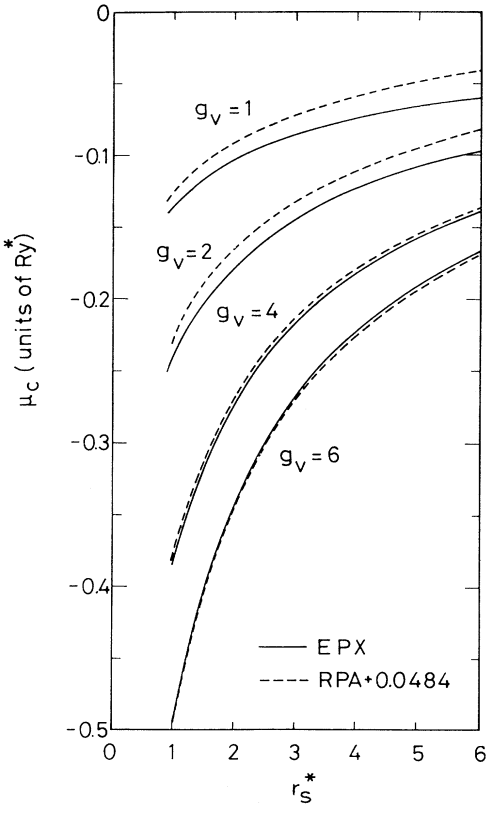


FIG. 7. Chemical potential shift due to the correlation effect $\mu_c$ in Ry* units as a function of $r_s^*$ for $g_v=1$, 2, 4, and 6. The dashed curves give the values of the sum of 0.0484 and $\mu_c$ in the RPA.

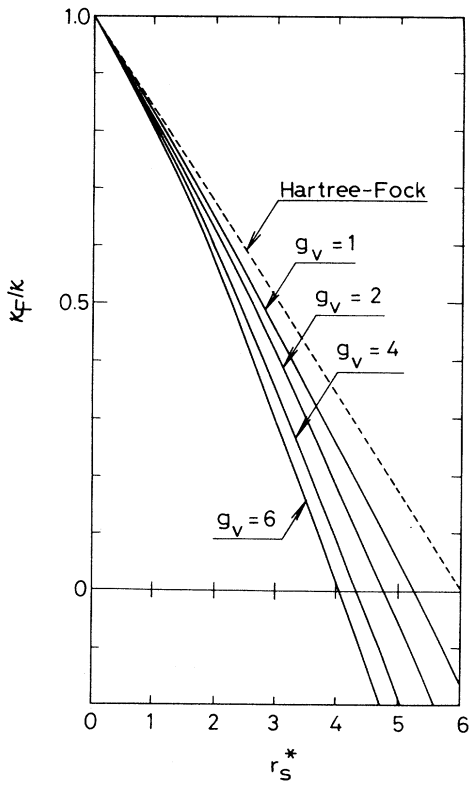


FIG. 8. Calculated results of the compressibility ratio $\kappa_F/\kappa$ as a function of $r_s^*$ for $g_v=1$, 2, 4, and 6, where $\kappa_F$ is the value in the noninteracting system. The values in the Hartree-Fock approximation are given by the dashed line.

TABLE III. Renormalization factor at the Fermi surface $z_F$ as a function of $r_s^*$ for $g_v=1$, 2, and 4. It is obtained from the magnitude of the discontinuity of $n(k)$ at $k=k_F$. Numbers in parentheses represent the results in the RPA as given by (6.5).

| $r_s^*$ | $g_v=1$ | $g_v=2$ | $g_v=4$ |
|---|---|---|---|
| 1 | 0.87(0.86) | 0.87(0.87) | 0.88(0.88) |
| 2 | 0.77(0.76) | 0.77(0.78) | 0.80(0.80) |
| 3 | 0.68(0.69) | 0.70(0.71) | 0.74(0.74) |
| 4 | 0.60(0.64) | 0.63(0.66) | 0.70(0.69) |
| 5 | 0.54(0.59) | 0.57(0.62) | 0.66(0.65) |

## VI. COMPARISON WITH THE RESULTS IN THE RPA

In this section we make $g_v$ large, while $r_s^*$ is fixed. According to (2.5), $r_s$ approaches zero in the large-$g_v$ limit. Thus the high-density expansion of Gell-Mann and Brueckner[17] is valid in this case and $\varepsilon_c$ is given only by the ring terms [Fig. 10(a)] and the second-order exchange diagram. The sum of the ring terms gives the energy in the RPA as

$$E_r=\tfrac{1}{2}\sum_{\mathbf{q}\,(\neq 0)}\int_{-\infty}^{\infty}\frac{d\Omega}{2\pi i}\{\ln[1+V(q)\Pi(q,\Omega)]-V(q)\Pi(q,\Omega)\}\ . \tag{6.1}$$

This is the sum of (4.2) and (4.3) with $\tilde{V}_l(q)$ replaced by $V(q)$. The second-order exchange diagram is given by

$$E_{\rm ex}^{(2)}=\frac{1}{2}\sum_{\mathbf{q}}\sum_{\mathbf{k},\sigma}\sum_{\mathbf{k}',\sigma'}\delta_{\sigma\sigma'}V(q)V(|\mathbf{k}'-\mathbf{k}-\mathbf{q}|)\frac{n_{\mathbf{k}\sigma}(1-n_{\mathbf{k}+\mathbf{q},\sigma})n_{\mathbf{k}'\sigma'}(1-n_{\mathbf{k}'-\mathbf{q},\sigma'})}{\Delta(\mathbf{k};\mathbf{q})+\Delta(\mathbf{k}';-\mathbf{q})}\ . \tag{6.2}$$

We can calculate the integral in (6.2) analytically[18] and obtain the value of 0.0484 Ry* per electron, which is independent of both $r_s^*$ and $g_v$. By comparing $(E_r+E_{\rm ex}^{(2)})/N$ with $\varepsilon_c$ in the EPX method, we find that for $g_v\geq 4$, they are very close as shown in Fig. 11. The same is true for $\mu_c$, as shown in Fig. 7. Since $E_r/N$ becomes much larger than $E_{\rm ex}^{(2)}/N$ for large $g_v$, $\varepsilon_c$ is almost given by the ring diagrams for $g_v\geq 4$. This indicates that the critical value of $g_v$ mentioned in Sec. I is 4 at least for $r_s^*<6$.

Now let us make a deeper investigation of the unexpectedly small value 4 for the critical $g_v$. In the usual perturbation-theoretic approach, the most important terms in the expansion series for $\varepsilon_c$ at large $g_v$ are the ring terms in Fig. 10(a), i.e., the diagrams with the maximum number of polarization bubbles in each order of $V(q)$. In Figs. 10(b)–10(d) we give all the leading correction diagrams in which the number of bubbles becomes smaller by one than that for the ring diagrams in each order of $V(q)$. These terms give a correction of the order $(2g_v)^{-1}$. In the second-

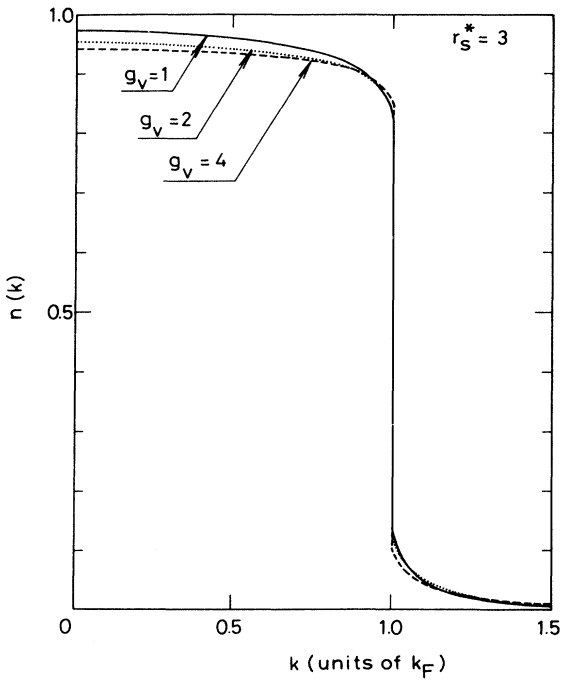


FIG. 9. Example of the calculated $n(k)$. The cases of $g_v=1$ (solid curve), 2 (dotted curve), and 4 (dashed curve) are considered at $r_s^*=3$.

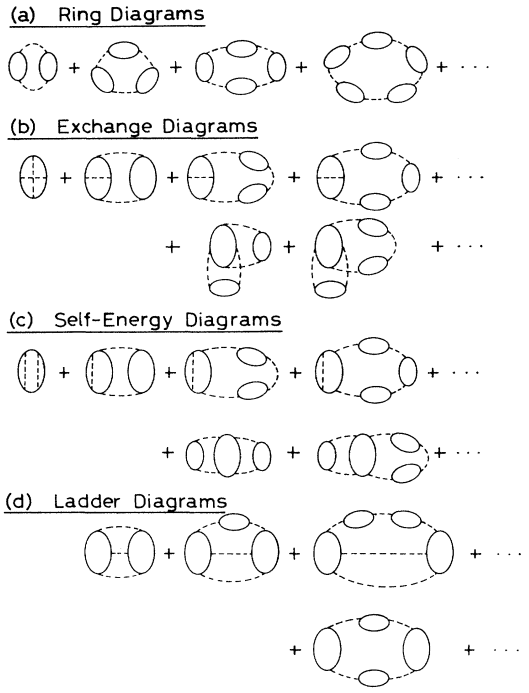


FIG. 10. Feynman diagrams for the ring terms given in (a) in which the number of bubbles becomes maximum in each order of $V(q)$. The next maximum number of bubbles is realized in the exchange terms (b), the self-energy terms (c), and the ladder terms (d).

order diagrams, the exchange term in Fig. 10(b) is already considered in (6.2), while the self-energy term in Fig. 10(c) vanishes exactly. Since the results in Fig. 11 show that there are no other large corrections to the RPA results, we have a strong indication that the sum of all the terms higher than second order in Figs. 10(b)–10(d) is very close to zero. This indication cannot be proven rigorously now, but we can give support to it by the calculation of third-order terms in which one of the bare interactions is replaced by the screened one to avoid divergence. The third-order exchange diagram $E_{\rm ex}^{(3)}$ is given by (4.7) with the following replacement:

$$\frac{\tilde{V}_l(q)}{\epsilon(q,\Omega)}\frac{V(q')}{[\epsilon(q',\Omega')]^2}\rightarrow\left[\frac{V(q)}{1+V(q)\Pi(q,\Omega)}-V(q)\right]V(q')\ . \tag{6.3}$$

This term can be evaluated in the same way as in (4.10). The third-order self-energy term $E_s^{(3)}$ can also be evaluated with a replacement similar to (6.3) in (4.11). The third-order ladder term $E_l^{(3)}$ is given by

$$\begin{aligned}E_l^{(3)}=&\tfrac{1}{6}\sum_{\mathbf{q},\mathbf{q}'}\sum_{\mathbf{k},\sigma}\sum_{\mathbf{k}',\sigma'}\int_{-\infty}^{\infty}\frac{d\Omega}{2\pi i}\int_{-\infty}^{\infty}\frac{d\Omega'}{2\pi i}\int_{-\infty}^{\infty}\frac{d\omega}{2\pi i}\int_{-\infty}^{\infty}\frac{d\omega'}{2\pi i}\frac{V(q)}{1+V(q)\Pi(q,\Omega)}\\&\times V(q')V(|\mathbf{q}'-\mathbf{q}|)G_{\mathbf{k}\sigma}(\omega)G_{\mathbf{k}+\mathbf{q},\sigma}(\omega+\Omega)G_{\mathbf{k}+\mathbf{q}',\sigma}(\omega+\Omega')G_{\mathbf{k}'\sigma'}(\omega')\\&\times[G_{\mathbf{k}'-\mathbf{q},\sigma'}(\omega'-\Omega)G_{\mathbf{k}-\mathbf{q}',\sigma'}(\omega'-\Omega')+G_{\mathbf{k}'+\mathbf{q},\sigma'}(\omega'+\Omega)G_{\mathbf{k}+\mathbf{q}',\sigma'}(\omega'+\Omega')]\ .\end{aligned} \tag{6.4}$$

Since the $\Omega$-dependent interaction cannot be treated for this term at present, we use the static approximation for $\Pi(q,\Omega)$. Then the integral in (6.4) can be performed in the same way as in (A5)–(A7). In Fig. 12(a) we show the results of $E_{\rm ex}^{(3)}$, $E_s^{(3)}$, and $E_l^{(3)}$ as a function of $r_s^*$ by the dashed curves for $g_v=1$. The sum of them (the solid curve) is almost a constant and close to zero. The same is true for other $g_v$ as shown in Fig. 12(b). Thus we may conclude that there is a strong cancellation among the terms of the exchange, self-energy, and ladder terms. As a result of this cancellation, the leading correction to the RPA terms in (6.1) is given only by (6.2). Note that such a cancellation does not seem to exit in the next correction terms of the order $(2g_v)^{-2}$, because $\varepsilon_c$ is different from the sum of (6.1) and (6.2) for $g_v=1$ and 2.

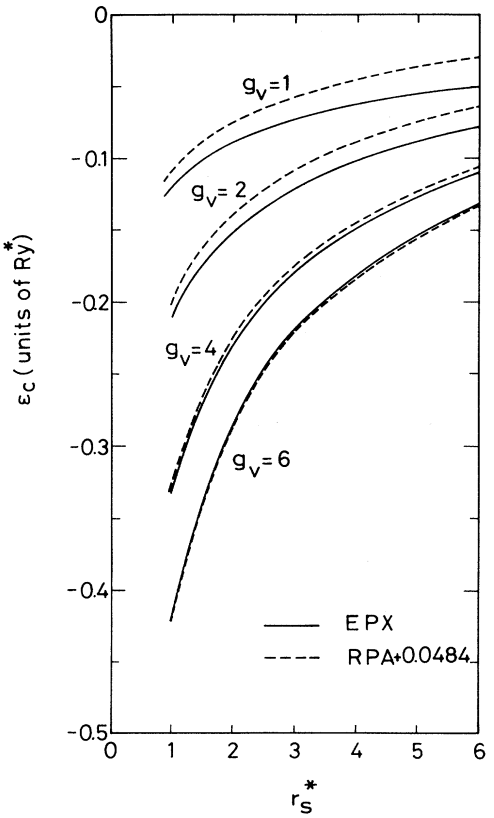


FIG. 11. Correlation energy $\varepsilon_c$ in our calculation (solid curves) compared with the sum of the RPA result (6.1) and 0.0484 Ry* (dashed curves) as a function of $r_s^*$ for $g_v=1$, 2, 4, and 6.

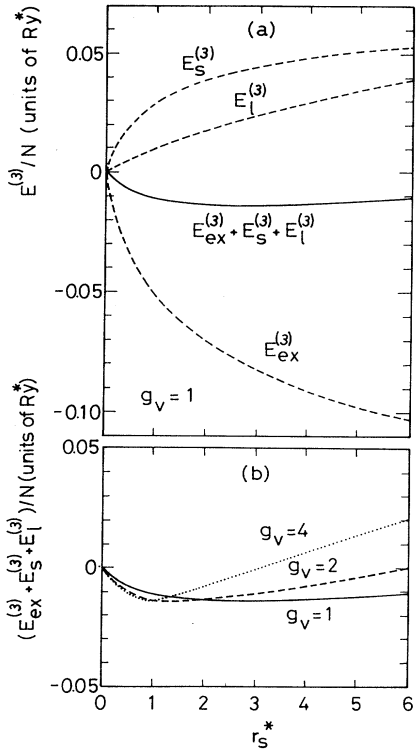


FIG. 12. (a) Calculated $r_s^*$ dependence of $E_{\rm ex}^{(3)}$, $E_s^{(3)}$, and $E_l^{(3)}$ for the case of $g_v=1$. They are given by the dashed curves, and their sum is plotted by the solid curve. (b) The sum of $E_{\rm ex}^{(3)}$, $E_s^{(3)}$, and $E_l^{(3)}$ as a function of $r_s^*$ for the cases of $g_v=1$, 2, and 4, which are, respectively, shown by the solid, dashed, and dotted curves.

Since it is a constant, (6.2) does not contribute to $\kappa$ given by (5.2). Thus $\kappa$ is determined completely only by the ring terms for $g_v \geq 4$. The same also seems to be true for $z_F$. This can be shown by the comparison of our results for $z_F$ with those in the RPA. When the important vertex corrections as given by the exchange and ladder diagrams are almost canceled by the self-energy corrections, the momentum distribution function is given by the sum of the ring diagrams without any self-energy corrections as in Fig. 13.[11,16] Then we obtain

$$z_F = \frac{1}{1-\partial\Sigma_{\rm RPA}(k_F,\omega)/\partial\omega} , \tag{6.5}$$

where $\omega$ is set equal to $k_F^2/2m^*$, and $\Sigma_{\rm RPA}(|\mathbf{k}|,\omega)$ is given by

$$\Sigma_{\rm RPA}(|\mathbf{k}|,\omega) = -\sum_{\mathbf{q}} \int_{-\infty}^{\infty} \frac{d\Omega}{2\pi i} G_{\mathbf{k}+\mathbf{q},\sigma}(\omega+\Omega) \frac{V(q)}{1+V(q)\Pi(q,\Omega)} . \tag{6.6}$$

In Table III the numbers in parentheses give the results of (6.5). Although the values in the EPX method are always very close to those of (6.5) for small $r_s^*$, it is true only for $g_v \geq 4$ for large $r_s^*$.

## VII. FERMION-BOSON CONVERSION AND VALLEY-POLARIZED STATES

In this section we change $g_v$, while the total number of electrons is fixed to $N$. Namely, we consider the total energy $E_0$ as a function of $g_v$ for a fixed value of $r_s$ instead of $r_s^*$. It is well known that at very low densities ($r_s \gg 1$), $E_0$ depends only on $r_s$, because the Coulomb interaction dominates over statistics. Thus $E_0$ is the same whether it is for the charged-boson system, the paramagnetic electron gas with the valley degeneracy $g_v$, or the totally polarized ferromagnetic electron gas. Here we take a step forward and show that for any $r_s$, $E_0$ changes smoothly from the value for the ferromagnetic electron gas at $g_v = \frac{1}{2}$ to the value for the charged-boson system at $g_v = \infty$ through the value for the paramagnetic electron gas at $g_v = 1$ as $g_v$ is increased.

Let us consider the high-density case ($r_s \ll 1$) first. For fermions, $E_0$ is given by the sum of $E_{\rm HF}$ and (6.1). In the large-$g_v$ limit, however, $E_{\rm HF}$ is zero. We also note that the $\Omega$ integral in (6.1) can be easily done, because the polarization function (4.5) has the form

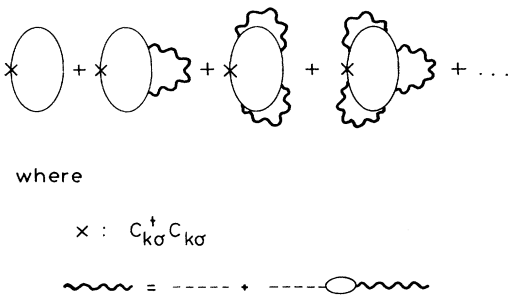


FIG. 13. Feynman diagrams for the momentum distribution function in the RPA without the self-energy corrections.

$$\Pi(q,i\Omega) = N\frac{2\varepsilon_{\mathbf{q}}}{\Omega^2+\varepsilon_{\mathbf{q}}^2} , \tag{7.1}$$

when each valley has at most one electron at the bottom for $2g_v \geq N$. Then we obtain $E_0$ in the large-$g_v$ limit as

$$E_0 = \tfrac{1}{2}\sum_{\mathbf{q}\,(\neq 0)} \{[\varepsilon_{\mathbf{q}}^2 + 2N\varepsilon_{\mathbf{q}}V(q)]^{1/2} - \varepsilon_{\mathbf{q}} - NV(q)\} . \tag{7.2}$$

This is nothing but the ground-state energy for the charged-boson system at high densities,[5] which was derived by the Bogoliubov method[17] with a condensation of a macroscopic number of particles at zero momentum. Thus $E_0$ for fermions is proven to approach the value for bosons at high densities with the increase of $g_v$. Note that the functional form of $E_0$ in terms of $r_s$ changes with $g_v$. For finite $g_v$, $E_0$ behaves like $0.0622 g_v \ln r_s$, while (7.2) leads to $-0.8031/r_s^{3/4}$.

For $r_s$ of the order of unity, we have numerical data of $E_0$ for various $g_v$ by combining the results for $\varepsilon_c$ in (5.1) with $E_{\rm HF}$. In Figs. 14(a)–14(c) we plot our results for $E_0$ at $r_s = 1$, 2, and 5 as a function of $g_v^{-1}$ by the crosses, together with those in the GFMC by the open circles for the charged-boson system at $g_v = \infty$, the paramagnetic electron gas at $g_v = 1$, and the ferromagnetic electron gas at $g_v = \frac{1}{2}$. (At $r_s = 1$ we used the values for the bosons and ferromagnetic phase given by the hypernetted-chain calculation of Zabolitzky[20] instead, because the GFMC data are not available for them.) The results in the Hartree-Fock approximation and RPA are also shown by the dashed and dotted curves, respectively. Clearly, all the data of $E_0$ with Fermi statistics converge to the result for the charged-boson system at each $r_s$ as $g_v$ is increased.

An unexpected fact in Fig. 14 is that even for $g_v$ as small as 10, $E_0$ is already close to that for the bosons. This may be explained as follows: In the interacting boson system, the particles occupy the states with finite momenta besides the condensation at zero momentum. If the average extent of the momentum distribution becomes larger than $k_F$, there is only a small difference in the correlation energy between the bosons and fermions. In terms of energies, the same condition can be stated that the interaction energy $1/r_s$ becomes larger than the

Fermi energy of each valley, $3.7g_v^{-2/3}r_s^{-2}$. This condition is rewritten as $g_v$ larger than $7r_s^{-3/2}$, which is of order 10 for $r_s$ of order unity.

For $r_s$ less than about 7.5, $E_0$ decreases monotonically with the increase of $g_v$, as shown in Fig. 14. Thus, at those densities, the most stable state is the one with the highest total degeneracy allowed for given $g_v$ and $N$. This means that the paramagnetic valley-unpolarized

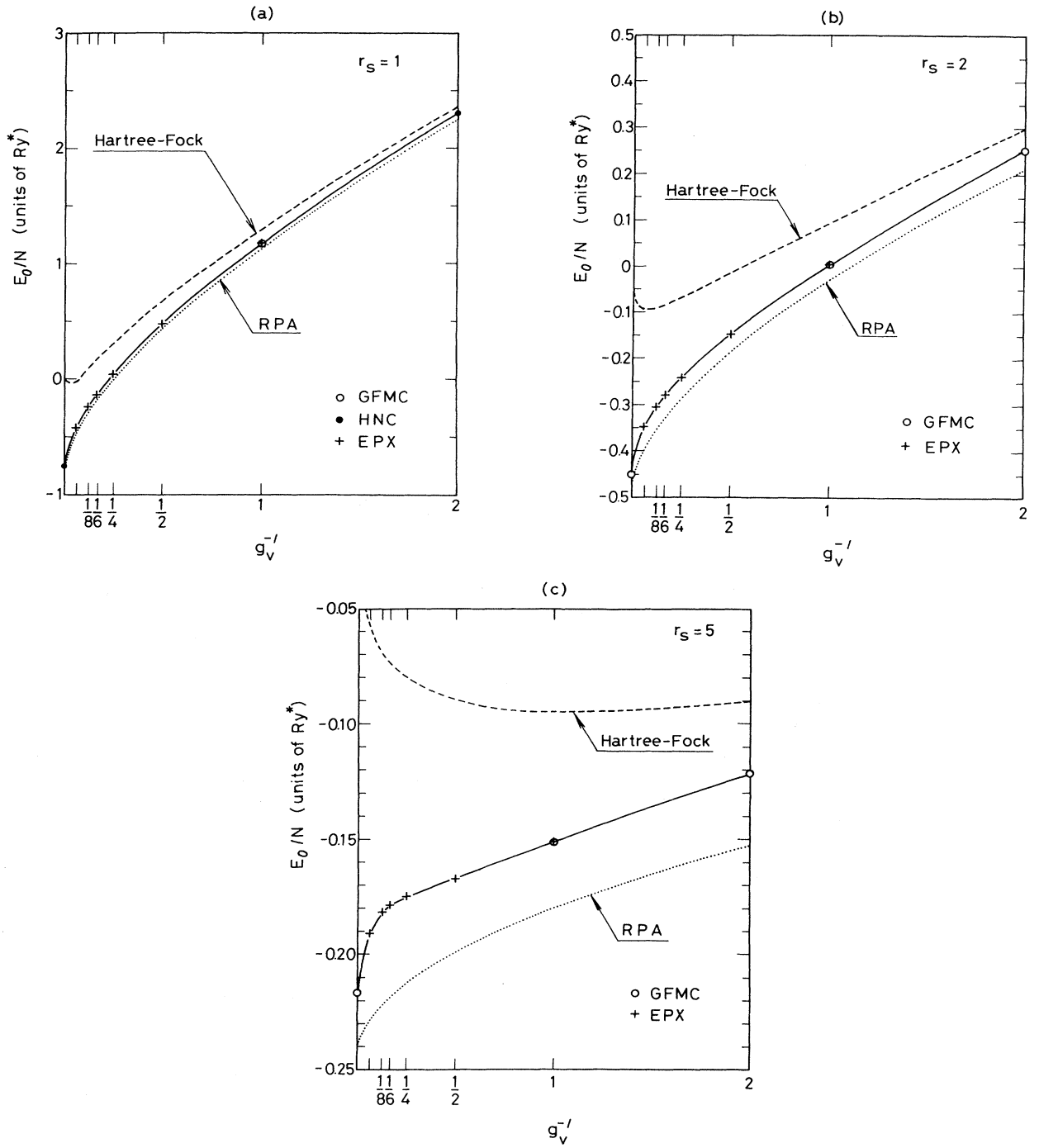


FIG. 14. Total energy per particle in Ry* units as a function of $g_v^{-1}$ at $r_s = 1$, 2, and 5 in (a), (b), an (c), respectively. The results are given by the crosses, and the solid curves are drawn as a guide to the eye. Those in the GFMC method (Ref. 1) for the charged-boson system at $g_v = \infty$, the paramagnetic electron gas at $g_v = 1$, and the ferromagnetic electron gas at $g_v = \frac{1}{2}$ are also shown by the open circles. [At $r_s = 1$, the results in the GFMC method are not available for bosons and ferromagnetic phase. Thus those in the hypernetted-chain (HNC) method of Zabolitzky (Ref. 20) are used instead. They are given by the solid circles.] For comparison, the results in the Hartree-Fock approximation and RPA are shown by the dashed and dotted curves, respectively.

state assumed in (3.1) has the lowest energy at the usual metallic densities. At lower densities, however, the situation is not so simple. In Fig. 15 we show the results for $E_0/N$ as a function of $g_v^{-1}$ at $r_s=10$, 20, and 50. The curve of $E_0$ has a local minimum at $g_v$ in the range from 1 to 2 and a maximum at $g_v$ from 6 to 10. This indicates that if the given $g_v$ is around the value to give the maximum of $E_0$, the ground state will not be valley unpolarized, but will be a valley-polarized state in which electrons go into only some of the valleys among several equivalent ones to reach the minimum of $E_0$ at a lower value of $g_v$. In particular, for $r_s$ larger than about 12, the local minimum of $E_0$ goes at $g_v$ equal to about 1. Thus, for those densities with a given $g_v$ less than about 10, either a paramagnetic single-valley or a ferromagnetic double-valley state will appear. These two states are degenerate because of the symmetry between spin and valley variables in our model Hamiltonian (2.1).

We admit that our results for $E_0$ in Fig. 15 at low densities are not so accurate as those in Fig. 14 at metallic densities. Thus the value 12 for the critical $r_s$ may not be so reliable. However, we believe that the qualitative behavior of $E_0$ as a function of $g_v$ is correct from the following considerations: According to the results in the GFMC method, we know that $E_0(g_v=\frac{1}{2})<E_0(g_v=1)>E_0(g_v=\infty)$ for $r_s\geq 75$. Thus $E_0$ certainly has a maximum at some value of $g_v$ at low enough densities. The existence of such a maximum leads to some kind of polarized states. Then the problem is whether the maximum in $E_0$ appears for $r_s$ much lower than 75. To answer that question, we note that the exchange effect is the driving force to make $E_0(g_v=\frac{1}{2})$ lower than $E_0(g_v=1)$. The same effect is also the driving force for the valley-polarized state. The correlation effect, on the other hand, works to destroy such polarized states, but its resisting force is not so strong in the partially polarized state such as the paramagnetic valley-polarized and the ferromagnetic double-valley ones compared to the ferromagnetic single-valley state, because the correlation energy is still large in the former case, while it is very small in the latter. Thus the partially polarized state will be realized at $r_s$ much lower than 75.

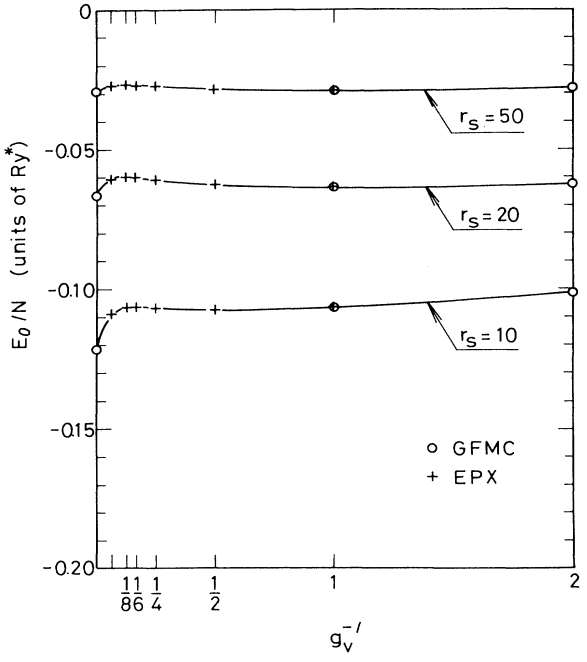


FIG. 15. Total energy per particle in Ry* units as a function of $g_v^{-1}$ at $r_s=10$, 20, and 50. The meanings of the symbols are the same as in Fig. 14.

## VIII. SUMMARY AND DISCUSSION

In a technical aspect this paper provides a detailed account of the improved version of the EPX method. Both the short- and long-range parts of the correlation are described accurately in terms of the two effective potentials $\tilde{V}_l$ and $\tilde{V}_s$. The approximations employed in the old version of Ref. 4 without any proofs are examined their validity. Many exchange terms neglected in Ref. 4 are considered explicitly, and all the important terms up to eighth order in $\tilde{V}_s$ are considered. Now the EPX method is shaped into a form that provides reliable results for the quasiparticle properties at the Fermi surface at metallic densities. We will develop a microscopic description of Landau's Fermi-liquid theory in this formalism in a future publication.

In a physical aspect we have investigated the correlation problem in the multivalley electron gas seriously. The valley degeneracy is shown to be a good parameter for converting the results of the ground-state energy for the fermions to those for bosons. Based on this conversion, the possibility of paramagnetic valley-polarized and ferromagnetic valley-unpolarized states is discussed. Those partially polarized states are found to occur much more easily than the totally polarized ferromagnetic state, though at usual metallic densities the paramagnetic valley-unpolarized state is found to be the ground state. In the paramagnetic valley-unpolarized state with $g_v\geq 4$ and $r_s^*<6$, the RPA is found to describe the correlation effect well. Because of a strong cancellation among the leading correction diagrams to the RPA, such a small critical value for $g_v$ is obtained.

The valley-unpolarized state was assumed in all the discussions of superconductivity in the multivalley electron gas.[6-8] In Refs. 6 and 8, the basic ingredient is either the intervalley scatterings or the intervalley pairing. Thus the question about the valley polarization is quite important. We need to discuss it with the electron-phonon interaction in addition to the Coulomb interaction. In the case of Ref. 8, we also need to consider the effect of the strong magnetic field. As for Ref. 7, on the other hand, the system is just the same as described in (2.1), and superconductivity was predicted to occur only with the Coulomb interaction if $r_s$ was larger than, for example, 2.2 for $g_v=6$. This value of $r_s$ is in the paramagnetic valley-unpolarized region, and the approximation employed in Ref. 7 was essentially the same as the RPA. Thus we may think that at least qualitatively the prediction that superconductivity will occur in the multivalley

electron gas is correct. As for the transition temperature $T_c$, however, we cannot expect much, because the valley-unpolarized state will be replaced by the valley-polarized state long before the maximum of $T_c$ around 1 K is achieved at very large $r_s$. Then the problem is reduced to that of superconductivity in the single-valley electron gas.[4] Thus the multivalley electron gas might not be so interesting from the viewpoint of the plasmon mechanism of superconductivity. From the viewpoint of the fermion-boson conversion, however, it still seems to provide an interesting problem. In the charged-boson system, we know definitely that superconductivity occurs with the Coulomb interaction because of the Bose condensation. Thus there must be some relation of this superconductivity to that in the electron gas. This will be discussed in the future, but in relation to this problem we point out the usefulness and feasibility of the Monte Carlo calculations for the low-density many-valley electron gas compared to the single-valley gas.

## ACKNOWLEDGMENTS

The author would like to thank T. Ando, M. Imada, and W. Kohn for useful discussions on the fermion-boson conversion.

## APPENDIX A: EXPLICIT EXPRESSIONS FOR SECOND-ORDER TERMS

An explicit expression for each diagram in Fig. 4 is given as follows. The terms in Fig. 4(a) are given by

$$E^{(2)}(H_0)=\frac{1}{2}\sum_{\mathbf{q}}\sum_{\mathbf{k},\sigma}\sum_{\mathbf{k}',\sigma'}[\bar{V}_s(q)\epsilon(q,0)-\delta_{\sigma\sigma'}\bar{V}_s(|\mathbf{k}'-\mathbf{k}-\mathbf{q}|)]\bar{V}_s(q)\frac{n_{\mathbf{k}\sigma}(1-n_{\mathbf{k}+\mathbf{q},\sigma})n_{\mathbf{k}'\sigma'}(1-n_{\mathbf{k}'-\mathbf{q},\sigma'})}{\Delta(\mathbf{k};\mathbf{q})+\Delta(\mathbf{k}';-\mathbf{q})}\ . \tag{A1}$$

The ring family [Fig. 4(b)] is obtained as

$$\begin{aligned}E_r^{(2)}(V)=\sum_{\mathbf{q}}\sum_{\mathbf{k},\sigma}\sum_{\mathbf{k}',\sigma'}\sum_{\mathbf{k}'',\sigma''}&\bar{V}_s(q)[V(q)\bar{V}_s(q)\epsilon(q,0)-\delta_{\sigma'\sigma''}\bar{V}(|\mathbf{k}'-\mathbf{k}''|)\bar{V}_s(q)\epsilon(q,0)\\&-2\delta_{\sigma\sigma'}\bar{V}(q)\epsilon(q,0)\bar{V}_s(|\mathbf{k}'-\mathbf{k}-\mathbf{q}|)+2\delta_{\sigma\sigma'}\delta_{\sigma'\sigma''}\bar{V}(|\mathbf{k}'-\mathbf{k}''|)\bar{V}_s(|\mathbf{k}'-\mathbf{k}-\mathbf{q}|)]\\&\times\frac{n_{\mathbf{k}\sigma}(1-n_{\mathbf{k}+\mathbf{q},\sigma})n_{\mathbf{k}'\sigma'}(1-n_{\mathbf{k}'-\mathbf{q},\sigma'})n_{\mathbf{k}''\sigma''}(1-n_{\mathbf{k}''-\mathbf{q},\sigma''})}{[\Delta(\mathbf{k};\mathbf{q})+\Delta(\mathbf{k}';-\mathbf{q})][\Delta(\mathbf{k};\mathbf{q})+\Delta(\mathbf{k}'';-\mathbf{q})]}\ .\end{aligned} \tag{A2}$$

The self-energy family [Fig. 4 (c)] is given by

$$\begin{aligned}E_s^{(2)}(V)=\sum_{\mathbf{q}}\sum_{\mathbf{k},\sigma}\sum_{\mathbf{k}',\sigma'}\sum_{\mathbf{k}'',\sigma''}&\delta_{\sigma'\sigma''}\bar{V}(|\mathbf{k}'-\mathbf{k}''|)\bar{V}_s(q)[\bar{V}_s(q)\epsilon(q,0)-\delta_{\sigma\sigma'}\bar{V}_s(|\mathbf{k}'-\mathbf{k}-\mathbf{q}|)]\\&\times\frac{n_{\mathbf{k}\sigma}(1-n_{\mathbf{k}+\mathbf{q},\sigma})n_{\mathbf{k}'\sigma'}(1-n_{\mathbf{k}'-\mathbf{q},\sigma'})(n_{\mathbf{k}''\sigma''}-n_{\mathbf{k}''-\mathbf{q},\sigma''})}{[\Delta(\mathbf{k};\mathbf{q})+\Delta(\mathbf{k}';-\mathbf{q})]^2}\ .\end{aligned} \tag{A3}$$

Finally, the ladder family [Fig. 4(d)] is composed of three terms:

$$E_l^{(2)}(V)=E_{ee}^{(2)}(V)+E_{hh}^{(2)}(V)+E_{eh}^{(2)}(V)\ , \tag{A4}$$

where

$$\begin{aligned}E_{ee}^{(2)}(V)=\tfrac{1}{2}\sum_{\mathbf{q},\mathbf{q}'}\sum_{\mathbf{k},\sigma}\sum_{\mathbf{k}',\sigma'}&\bar{V}_s(q)\bar{V}_s(q')[\bar{V}(|\mathbf{q}'-\mathbf{q}|)-\delta_{\sigma\sigma'}\bar{V}(|\mathbf{k}'-\mathbf{k}-\mathbf{q}-\mathbf{q}'|)]\\&\times\frac{n_{\mathbf{k}\sigma}(1-n_{\mathbf{k}+\mathbf{q},\sigma})(1-n_{\mathbf{k}+\mathbf{q}',\sigma})n_{\mathbf{k}'\sigma'}(1-n_{\mathbf{k}'-\mathbf{q}\sigma'})(1-n_{\mathbf{k}'-\mathbf{q}',\sigma'})}{[\Delta(\mathbf{k};\mathbf{q})+\Delta(\mathbf{k}';-\mathbf{q})][\Delta(\mathbf{k};\mathbf{q}')+\Delta(\mathbf{k}';-\mathbf{q}')]}\ .\end{aligned} \tag{A5}$$

$$\begin{aligned}E_{hh}^{(2)}(V)=\tfrac{1}{2}\sum_{\mathbf{q},\mathbf{q}'}\sum_{\mathbf{k},\sigma}\sum_{\mathbf{k}',\sigma'}&\bar{V}_s(q)\bar{V}_s(q')[\bar{V}(|\mathbf{q}'-\mathbf{q}|)-\delta_{\sigma\sigma'}\bar{V}(|\mathbf{k}'-\mathbf{k}-\mathbf{q}-\mathbf{q}'|)]\\&\times\frac{(1-n_{\mathbf{k}\sigma})n_{\mathbf{k}+\mathbf{q},\sigma}n_{\mathbf{k}+\mathbf{q}',\sigma}(1-n_{\mathbf{k}'\sigma'})n_{\mathbf{k}'-\mathbf{q},\sigma'}n_{\mathbf{k}'-\mathbf{q}',\sigma'}}{[\Delta(\mathbf{k};\mathbf{q})+\Delta(\mathbf{k}';-\mathbf{q})][\Delta(\mathbf{k};\mathbf{q}')+\Delta(\mathbf{k}';-\mathbf{q}')]}\ ,\end{aligned} \tag{A6}$$

and

$$\begin{aligned}E_{eh}^{(2)}(V)=-\sum_{\mathbf{q},\mathbf{q}'}\sum_{\mathbf{k},\sigma}\sum_{\mathbf{k}',\sigma'}&\bar{V}_s(q)\bar{V}_s(q')[\bar{V}(|\mathbf{q}'-\mathbf{q}|)-\delta_{\sigma\sigma'}\bar{V}(|\mathbf{k}'-\mathbf{k}|)]\\&\times\frac{(1-n_{\mathbf{k}\sigma})n_{\mathbf{k}+\mathbf{q},\sigma}n_{\mathbf{k}+\mathbf{q}',\sigma}n_{\mathbf{k}'\sigma'}(1-n_{\mathbf{k}'-\mathbf{q},\sigma'})(1-n_{\mathbf{k}'-\mathbf{q}',\sigma'})}{[\Delta(\mathbf{k};\mathbf{q})+\Delta(\mathbf{k}';-\mathbf{q})][\Delta(\mathbf{k};\mathbf{q}')+\Delta(\mathbf{k}';-\mathbf{q}')]}\ .\end{aligned} \tag{A7}$$

## APPENDIX B: EXPLICIT EXPRESSIONS FOR HIGHER-ORDER TERMS

The higher-order ring family considered in this paper is the sum of $E_r^{(2n-1)}(V)$, $E_r^{(2n)}(V)$, and $E_r^{(2n)}(H_0)$ with $n$ from 2 to 4. These terms are, respectively, given as

$$E_r^{(2n-1)}(V)=-\sum_{\mathbf{q}}\sum_{\mathbf{k}_1,\sigma_2}\cdots\sum_{\mathbf{k}_{2n},\sigma_{2n}}[\bar{V}_s(q)]^{2n-2}[\epsilon(q,0)]^{2n-4}$$
$$\times\{V(q)\bar{V}_s(q)[\epsilon(q,0)]^2-\delta_{\sigma_1\sigma_{2n}}\bar{V}(|\mathbf{k}_1-\mathbf{k}_{2n}+\mathbf{q}|)\bar{V}_s(q)[\epsilon(q,0)]^2-(2n-1)\delta_{\sigma_1\sigma_2}V(q)\bar{V}_s(|\mathbf{k}_1-\mathbf{k}_2+\mathbf{q}|)$$
$$+\delta_{\sigma_1\sigma_2}\delta_{\sigma_1\sigma_{2n}}[2n-3+2\epsilon(q,0)]\bar{V}(|\mathbf{k}_1-\mathbf{k}_{2n}+\mathbf{q}|)\bar{V}_s(|\mathbf{k}_1-\mathbf{k}_2+\mathbf{q}|)\}$$
$$\times\frac{n_{\mathbf{k}_1\sigma_1}(1-n_{\mathbf{k}_1+\mathbf{q},\sigma_1})n_{\mathbf{k}_2\sigma_2}(1-n_{\mathbf{k}_2-\mathbf{q},\sigma_2})\cdots n_{\mathbf{k}_{2n}\sigma_{2n}}(1-n_{\mathbf{k}_{2n}-\mathbf{q},\sigma_{2n}})}{[\Delta(\mathbf{k}_1;\mathbf{q})+\Delta(\mathbf{k}_2;-\mathbf{q})][\Delta(\mathbf{k}_2;-\mathbf{q})+\Delta(\mathbf{k}_3;\mathbf{q})]\cdots[\Delta(\mathbf{k}_{2n-1};\mathbf{q})+\Delta(\mathbf{k}_{2n};-\mathbf{q})]}\ , \tag{B1}$$

$$E_r^{(2n)}(V)=\sum_{\mathbf{q}}\sum_{\mathbf{k}_1,\sigma_1}\cdots\sum_{\mathbf{k}_{2n+1},\sigma_{2n+1}}[\bar{V}_s(q)]^{2n-1}[\epsilon(q,0)]^{2n-3}$$
$$\times\{V(q)\bar{V}_s(q)[\epsilon(q,0)]^2-\delta_{\sigma_1\sigma_{2n+1}}\bar{V}(|\mathbf{k}_1-\mathbf{k}_{2n+1}|)\bar{V}_s(q)[\epsilon(q,0)]^2-2n\delta_{\sigma_1\sigma_2}V(q)\bar{V}_s(|\mathbf{k}_1-\mathbf{k}_2+\mathbf{q}|)$$
$$+\delta_{\sigma_1\sigma_2}\delta_{\sigma_1\sigma_{2n+1}}[2n-2+2\epsilon(q,0)]\bar{V}(|\mathbf{k}_1-\mathbf{k}_{2n+1}|)\bar{V}_s(|\mathbf{k}_1-\mathbf{k}_2+\mathbf{q}|)\}$$
$$\times\frac{n_{\mathbf{k}_1\sigma_1}(1-n_{\mathbf{k}_1+\mathbf{q},\sigma_1})n_{\mathbf{k}_2\sigma_2}(1-n_{\mathbf{k}_2-\mathbf{q},\sigma_2})\cdots n_{\mathbf{k}_{2n+1}\sigma_{2n+1}}(1-n_{\mathbf{k}_{2n+1}+\mathbf{q},\sigma_{2n+1}})}{[\Delta(\mathbf{k}_1;\mathbf{q})+\Delta(\mathbf{k}_2;-\mathbf{q})][\Delta(\mathbf{k}_2;-\mathbf{q})+\Delta(\mathbf{k}_3;\mathbf{q})]\cdots[\Delta(\mathbf{k}_{2n};-\mathbf{q})+\Delta(\mathbf{k}_{2n+1};\mathbf{q})]}\ , \tag{B2}$$

and

$$E_r^{(2n)}(H_0)=\tfrac{1}{2}\sum_{\mathbf{q}}\sum_{\mathbf{k}_1,\sigma_1}\cdots\sum_{\mathbf{k}_{2n},\sigma_{2n}}[\bar{V}_s(q)]^{2n-2}[\epsilon(q,0)]^{2n-4}$$
$$\times\{[\bar{V}_s(q)]^2[\epsilon(q,0)]^3-\delta_{\sigma_1\sigma_2}[2n-2+2\epsilon(q,0)]\epsilon(q,0)\bar{V}_s(q)\bar{V}_s(|\mathbf{k}_1-\mathbf{k}_2+\mathbf{q}|)$$
$$+\delta_{\sigma_1\sigma_2}\delta_{\sigma_1\sigma_{2n}}[2n-3+2\epsilon(q,0)]\bar{V}(|\mathbf{k}_1-\mathbf{k}_{2n}+\mathbf{q}|)\bar{V}_s(|\mathbf{k}_1-\mathbf{k}_2+\mathbf{q}|)\}$$
$$\times\frac{n_{\mathbf{k}_1\sigma_1}(1-n_{\mathbf{k}_1+\mathbf{q},\sigma_1})n_{\mathbf{k}_2\sigma_2}(1-n_{\mathbf{k}_2-\mathbf{q},\sigma_2})\cdots n_{\mathbf{k}_{2n}\sigma_{2n}}(1-n_{\mathbf{k}_{2n}-\mathbf{q},\sigma_{2n}})}{[\Delta(\mathbf{k}_1;\mathbf{q})+\Delta(\mathbf{k}_2;-\mathbf{q})][\Delta(\mathbf{k}_2;-\mathbf{q})+\Delta(\mathbf{k}_3;\mathbf{q})]\cdots[\Delta(\mathbf{k}_{2n-1};\mathbf{q})+\Delta(\mathbf{k}_{2n};-\mathbf{q})]}\ . \tag{B3}$$

Similarly, the higher-order self-energy term is given by

$$E_s^{(2n)}(V)=\sum_{\mathbf{q}}\sum_{\mathbf{k}_1,\sigma_1}\cdots\sum_{\mathbf{k}_{2n},\sigma_{2n}}[\bar{V}_s(q)]^{2n-2}[\epsilon(q,0)]^{2n-4}(\varepsilon^{(F)}_{\mathbf{k}_1\sigma_1}-\varepsilon^{(F)}_{\mathbf{k}_1+\mathbf{q},\sigma_1})$$
$$\times\{[\bar{V}_s(q)]^2[\epsilon(q,0)]^3-\delta_{\sigma_1\sigma_2}[2n-2+2\epsilon(q,0)]\epsilon(q,0)\bar{V}_s(q)\bar{V}_s(|\mathbf{k}_1-\mathbf{k}_2+\mathbf{q}|)$$
$$+\delta_{\sigma_1\sigma_2}\delta_{\sigma_1\sigma_{2n}}[2n-3+2\epsilon(q,0)]\bar{V}(|\mathbf{k}_1-\mathbf{k}_{2n}+\mathbf{q}|)\bar{V}_s(|\mathbf{k}_1-\mathbf{k}_2+\mathbf{q}|)\}$$
$$\times\frac{n_{\mathbf{k}_1\sigma_1}(1-n_{\mathbf{k}_1+\mathbf{q},\sigma_1})n_{\mathbf{k}_2\sigma_2}(1-n_{\mathbf{k}_2-\mathbf{q},\sigma_2})\cdots n_{\mathbf{k}_{2n}\sigma_{2n}}(1-n_{\mathbf{k}_{2n}-\mathbf{q},\sigma_{2n}})}{[\Delta(\mathbf{k}_1;\mathbf{q})+\Delta(\mathbf{k}_2;-\mathbf{q})]\cdots[\Delta(\mathbf{k}_{2n-1};\mathbf{q})+\Delta(\mathbf{k}_{2n};-\mathbf{q})][\Delta(\mathbf{k}_{2n};-\mathbf{q})+\Delta(\mathbf{k}_1;\mathbf{q})]}\ , \tag{B4}$$

where

$$\varepsilon^{(F)}_{\mathbf{k}\sigma}=\sum_{\mathbf{k}'}\bar{V}(|\mathbf{k}-\mathbf{k}'|)n_{\mathbf{k}'\sigma}\ . \tag{B5}$$


[1]D. M. Ceperley and B. J. Alder, Phys. Rev. Lett. **45**, 566 (1980).
[2]K. Emrich and J. G. Zabolitzky, Phys. Rev. B **30**, 2049 (1984).
[3]Y. Takada, Phys. Rev. B **35**, 6923 (1987).
[4]Y. Takada, Phys. Rev. B **37**, 155 (1988).
[5]L. L. Foldy, Phys. Rev. **124**, 649 (1961); K. A. Brueckner, *ibid.* **156**, 204 (1967); E. Feenberg, *Theory of Quantum Fluids* (Academic, New York, 1969); E. A. Nosal and W. T. Grandy, Jr., Ann. Phys. (N.Y.) **55**, 1 (1969).
[6]M. L. Cohen, Phys. Rev. **134**, A511 (1964).
[7]Y. Takada, J. Phys. Soc. Jpn. **45**, 786 (1978).
[8]M. Rasolt, Phys. Rev. Lett. **58**, 1482 (1987).
[9]J. Goldstone, Proc. R. Soc. London Ser. A **239**, 267 (1957).
[10]Y. Takada, Phys. Rev. A **28**, 2417 (1983).
[11]T. M. Rice, Ann. Phys. (N.Y.) **31**, 100 (1965).
[12]H. Yasuhara, Solid State Commun. **11**, 1481 (1972).

[13]K. S. Singwi, M. P. Tosi, R. H. Land, and A. Sjölander, Phys. Rev. **176**, 589 (1968).
[14]S. H. Vosko, L. Wilk, and M. Nusair, Can. J. Phys. **58**, 1200 (1980).
[15]L. L. Foldy, Phys. Rev. B **3**, 3472 (1971); **17**, 4889 (1978).
[16]Y. Takada and H. Yasuhara (unpublished).
[17]M. Gell-Mann and K. A. Brueckner, Phys. Rev. **106**, 364 (1957).
[18]L. Onsager, L. Mittag, and M. J. Stephen, Ann. Phys. (N.Y.) **18**, 71 (1966).
[19]N. N. Bogoliubov, J. Phys. (U.S.S.R.) **11**, 23 (1947).
[20]J. G. Zabolitzky, Phys. Rev. B **22**, 2353 (1980).